Numerical study on the effect of guide vane opening and draft tube outlet pressure on cavitation in Kaplan turbine

DOI : 10.36909/jer.17267

Brijkishore*, Ruchi Khare, Vishnu Prasad

Maulana Azad National Institute of Technology, Bhopal, 462003, Madhya Pradesh, India.

* Corresponding Author: brijkishore844@gmail.com

ABSTRACT

The variations in electricity demand and site conditions like mass flow rate and net head, force the turbines to operate under off-design conditions. This increases cyclic loading in stationary and rotating components and severe cavitation in low head turbines like Kaplan turbine. The present analysis aims to examine the influence of various operating conditions on hydraulic efficiency and cavitation characteristics using ANSYS CFX. The stages of cavitation development in the runner are extensively studied for different operating conditions. The key point of present work is the critical analysis of various flow parameters for cavitating and non-cavitating conditions. The value of critical cavitation factor is found to increase from 0.34 to 0.61 with an increase in guide vane opening from 35º to 60º. The blade loading and flow parameters are found to be affected due to changes in guide vane opening and cavitation. The computed results are validated with the experimental model testing results and found to bear close comparison.

Keywords: Cavitation; Computational Fluid Dynamics (CFD); Hydraulic efficiency; Kaplan turbine; Off-design operating conditions.

INTRODUCTION

Hydraulic turbines are designed specifically for the particular head, flow rate and speed; however, the fluctuations in reservoir levels and electricity demand force the turbines to

operate at the off-design head and flow rates values (Celebioglu et al., 2017). The development of undesirable flow patterns due to such operating conditions leads to pressure fluctuations and cavitation phenomena and this affects the power output and hydraulic efficiency (Brijkishore et al., 2021). The hydraulic efficiency of turbine is calculated using the expression;

$$\eta_H = \frac{T\omega}{(P_{inlet} - P_{outlet})Q} * 100 \quad (1)$$

Where, Q, ω and T, and are the mass flow rate, angular speed of turbine shaft and torque, respectively. P_{inlet} and P_{outlet} are the total pressure at inlet and outlet, respectively.

Cavitation is an unsteady, three-dimensional, discontinuous or periodic, complex and dynamic phase transition phenomenon in hydraulic reaction turbines. The design fault and improper setting of turbines lead to the formation of vapour bubbles due to falls in localized pressure below the vapour pressure of water at a constant temperature. The collapse of these vapour bubbles in high-pressure zone leads to cavitation (Zhang et al., 2018). The minimum pressure inside the flow passage of water should not be less than the vapour pressure of water to avoid cavitation (Celebioglu et al., 2017).

Prof. Dietrich Thomas proposed a dimensionless number called the Thoma cavitation factor. It is commonly used to assess the cavitation characteristics in the hydraulic turbine. The Thoma cavitation factor is also termed as σ_{plant} or $\sigma_{installation}$, which is used to identify the particular zone under which the turbine may operate cavitation-free. The Thoma cavitation factor can be evaluated by the expression (Lal, 2011);

$$\sigma = \frac{\left(\frac{P_{atm} - P_v}{\rho g}\right) - H_s}{H} \quad (2)$$

Where, P_{atm} , P_v , H_s and H are the average atmospheric and vapour pressure of water, static suction head of turbine, net head of turbine respectively. Cavitation characteristics of hydraulic turbine are assessed by “sigma curve”. The sigma curve is determined by varying the pressure

at the draft tube outlet (Kamal et al., 2021). The various investigation has been carried out to better understand the scope of CFD for the numerical investigation of cavitation in hydraulic turbines and are summarized in Table 1. The steady and unsteady analyses were performed by various researchers as per the requirements using the Reynolds-averaged Navier-Stoke (RANS) and Unsteady Reynolds-averaged Navier-Stoke (URANS) equations, respectively.

Table 1. Summary of the numerical investigation of cavitation on Kaplan turbine.

Authors	**Solver code, Turbulence and Cavitation model**	**Objectives**	**Findings/Remarks**
(Nennemann and Vu, 2007)	CFX, SST, Rayleigh Plesset	Cavitation prediction on the blade surface and discharge ring.	Understanding of the physics behind the discharge ring and tip gap cavitation.
(Weili et al., 2010)	CFX	Cavitation characteristic under sediment flow conditions.	Cavitation in silt flow is more serious than in pure water
(Motycak et al., 2012)	CFX, k-ε, Rayleigh Plesset	Analysis and prevention of tip vortex cavitation and pitting effect on the blade surface.	The tip vortex cavitation was reduced by changing the deflection of blade camber line, reducing the tip clearance and providing anti-cavity lip.
(Kumar and Bhingole, 2015)	CFX, SST k-ω, Rayleigh Plesset	Combined effect of cavitation and silt erosion.	The possibility of cavitation increases with the appearance of silt concentration.
(Jošt et al., 2015)	CFX, SST, Zwart	To develop methods for predicting cavitation and performance optimization.	There was a small difference between the standard and calibrated results of Zwart mass transfer model.
(Shamsuddeen et al., 2020)	CFX, SST, Rayleigh Plesset	Cavitation reduction by anti-cavity fin installation.	Cavitation decreased at the leading edge. Modification of ACF shape at the trailing edge

			was recommended to avoid the runner blade damage.

A lot of investigation has been performed to determine the cavitation characteristics of Kaplan turbine. Based on the previous studies, it has been revealed that the critical analysis of various flow parameters has not been investigated for cavitating and non-cavitating conditions. The flow visualizations across the surface of runner blades and different cavitation stages in the runner have also not been examined in previous studies of Kaplan turbine.

In the present numerical simulation, the assessment of cavitation characteristics of Kaplan turbine has been carried out for different operating conditions using ANSYS CFX. The development of cavitation stages in the runner is extensively studied for various operating regimes. The present work highlights the critical analysis of various flow parameters for cavitating and non-cavitating conditions.

RESEARCH METHODOLOGY

The present methodology is divided into four steps. The first step is to prepare component-wise the 3-D geometry of the complete flow passage. The second step is to generate mesh of each component of the geometry. The boundary conditions are specified as per the operating regime of turbine in the third step. The last step is flow simulation in the turbine space and to obtain the required results in the post-processor.

The geometrical configuration of Kaplan turbine is a vertical axis turbine with a single pier elbow type draft tube. The runner diameter of model Kaplan turbine is 400mm and it is tested under a head of 10m. The computational flow domain of Kaplan turbine has been developed using Unigraphics NX and ANSYS ICEM CFD software. The domain consists of a single pier elbow type draft tube, a runner with 4 blades, a distributor with 28 guide vanes, a stay ring with 12 stay vanes and a spiral casing. Figure 1 illustrates the assembly of complete Kaplan turbine.

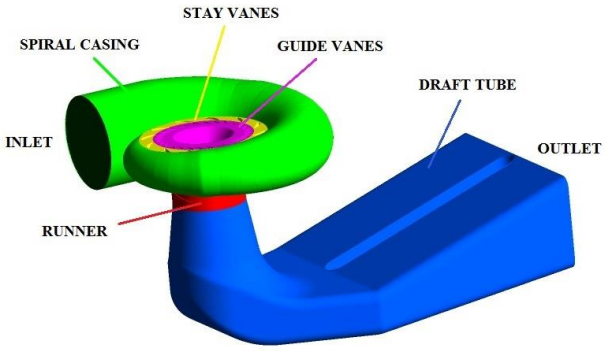

Figure 1. Complete assembly of Kaplan turbine

Grid or mesh generation of the 3D computational flow domain is the subsequent step after geometric model development. In the present investigation, ANSYS ICEM mesh module has been used for grid generation. The hybrid mesh with tetrahedral and hexahedral mesh elements and prism layer have been used in the present numerical simulation to capture the turbulent flow phenomenon. The prism layers have been created around the guide vanes, runner blade surfaces and the draft tube wall to resolve the boundary layer near the wall to get higher accuracy.

The details of mesh generation parameters and the optimum grid size after the grid independency test (GIT) are summarized in Table 2. Figure 2 represents the meshing of different components. The recommended values are between 20 and 200 for automated wall features (Teran et al., 2016). The Y^+ value of the runner is limited to about 40-185, which is the suitable range for automated wall features in the boundary layer for the turbulence model used. The quality of mesh generation determines the accuracy of the result and the convergence of numerical solutions (Saini and Saini, 2020). As per the definition followed by ANSYS ICEM mesh module tool, aspect ratio, skewness, orthogonal quality and element quality must be close to 1 for good quality mesh. In this study, the mean values of aspect ratio, skewness, orthogonal quality and element quality are 0.8878, 0.9399, 0.9274 and 0.8878 respectively.

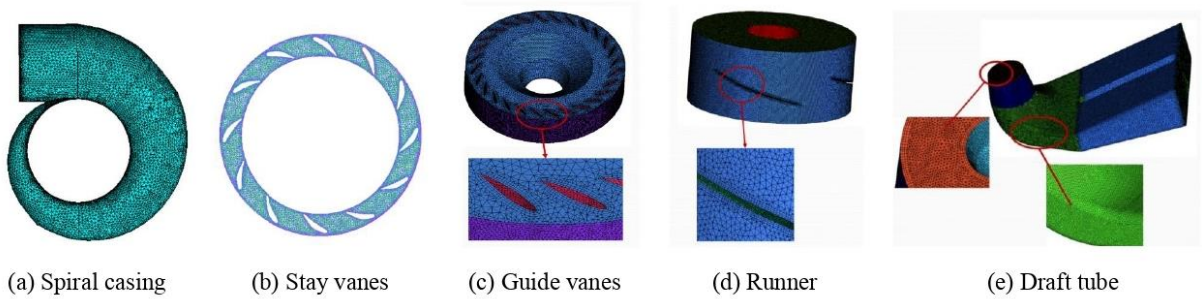

Figure 2. Mesh of different components

Table 2. Mesh details of different components of Kaplan turbine

Components	Number of nodes	Number of elements	Types of mesh and element
Spiral casing	205403	1039283	Unstructured (Tetrahedral)
Stay vanes	350896	1745496	Unstructured (Tetrahedral)
Guide vanes	519902	1888430	Unstructured and structured (Tetrahedral and hexahedral or prism)
Runner	762354	4333090	Unstructured and structured (Tetrahedral and hexahedral or prism
Draft tube (DT)	275410	1041215	Unstructured and structured (Tetrahedral and hexahedral or prism)
Complete assembly	2113965	10047514	

The grid independence test is essential for optimizing the grid size for numerical flow analysis. It was done by carrying out a number of simulations with different grid sizes. Figure 3 shows a variation in hydraulic efficiency with the number of nodes. The grid independence test was done for five different combinations of nodes to select the optimum grid size. It is found that the number of nodes 2113965 provides the minimum losses in the net head, power output and hydraulic efficiency and hence 2113965 nodes were considered for all the flow simulations.

The performance of numerical simulation of turbine mainly depends on the applied boundary conditions. Hence, the boundary conditions should be appropriately used to get the realistic flow simulation through the turbine (Brijkishore et al., 2020; Tiwari et al., 2020). The applied boundary conditions are the mass flow rate at the inlet section of spiral casing and average static pressure at the outlet section of draft tube. The experimental results are taken from Hydraulic

Machines Research and Testing Laboratory, MANIT Bhopal. The boundary conditions and experimental model test results are mentioned in Table 3.

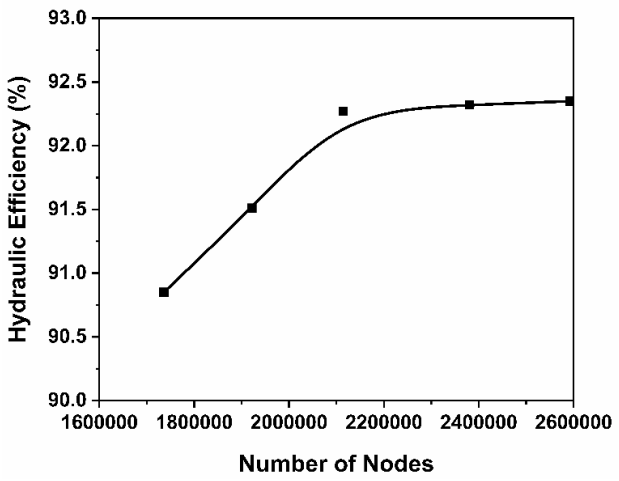

Figure 3. Grid independency test for the different number of nodes

In the present cavitation analysis, the mass flow rate is computed to match the experimental values of unit speed and unit discharge and specified at the spiral casing inlet as inlet boundary conditions. The average static pressure at the draft tube outlet is varied from 0.1 to 1 atm for outlet boundary conditions, as shown in Table 4.

Table 3. Experimental results for the validation of CFD results

GVO (º)	Unit discharge Q_{11} (l/s)	Unit speed N_{11} (rpm)	Experimental efficiency (%)	Critical cavitation factor (σ_c)
35º	1008	134	91.59	0.37
40º	1107	146	92.06	0.42
50º	1290	171	91.10	0.55
60º	1440	192	88.3	0.65

The appropriate turbulence model selection is important for the proper assessment of cavitation at design and off-design operating conditions. It is found from the literature survey that the two-equation based SST k-ω model is the most suitable turbulence model for the present study because it increases the accuracy of numerical flow prediction during adverse pressure gradient and separation of boundary layer (Brijkishore et al., 2020; Singh et al., 2021).

Table 4. Boundary conditions applied for cavitation analysis

GVO (º)	**Mass flow rate at the inlet of spiral casing (kg/s)**	**Average static pressure variation at the outlet of DT (atm)**
35º	556	0.1-1
40º	560	0.1-1
50º	558	0.1-1
60º	554	0.1-1
Reference pressure		0 atm
Rotational speed of the runner		1155 rpm

The governing equations consist of Reynolds-averaged Navier-Stoke (RANS) equations and Rayleigh Plesset cavitation model equation (two-phase cavitation model equation) (Liu et al., 2016). The Reynolds-averaged Navier-Stokes (RANS) equations are solved using the homogeneous two-phase mixture model. In the framework of homogeneous mixture model, the conservative mass and momentum equations are as follows (Shamsuddeen et al., 2020);

$$\frac{\partial \rho_m}{\partial t} + \frac{\partial (\rho_m u_i)}{\partial x_i} = \dot{m}_\alpha \tag{3}$$

$$\frac{\partial (\rho_m u_i)}{\partial t} + \frac{\partial (\rho_m u_i u_j)}{\partial x_j} = \frac{\partial p}{\partial x_i} + \frac{\partial (\tau_{ij})}{\partial x_j} + \rho_m \alpha_v g \tag{4}$$

Where $\dot{m}_\alpha$, u_i, ρ_m, p, α_v, τ_{ij} and g represent the phase mass generation rate (kg/m^{3}s), Cartesian velocity components (m/s), flow domain pressure (N/m^2), vapour volume fraction, stress tensor components and gravitational acceleration. The following transport equation for the water vapour mass transfer is established to define the phase change under cavitation conditions (Geng et al., 2020; Zhang et al., 2015);

$$\frac{\partial (\alpha_v \rho_v)}{\partial t} + \frac{\partial (\alpha_v \rho_v u_i)}{\partial x_j} = \dot{m} \tag{5}$$

The term $\dot{m}$ represents the mass transfer rate between the water and water vapour phases, which depends on the cavitation model used. In this work, the rate of vapour formation is determined using the Rayleigh-Plesset cavitation model.

RESULTS AND DISCUSSIONS

The numerical flow simulation of turbine flow passage has been carried out at different operating conditions. The problems of existing turbines are examined through turbine efficiency curves, blade loading, sigma curves, flow parameters, pressure distributions and water vapour volume fraction.

Validation of computational results with experimental

Validation is the most crucial step for ensuring the authenticity of CFD results. In this work, validation of numerical simulation has been performed at different operating conditions. The hydraulic efficiency of numerical simulations is closely matched with the experimental results at 35º, 40º, 50º and 60º GVO. The comparison of CFD results with the experimental model-tested results shows that the variation pattern of hydraulic efficiency is similar for both computational and experimental, as illustrated in Figure 4.

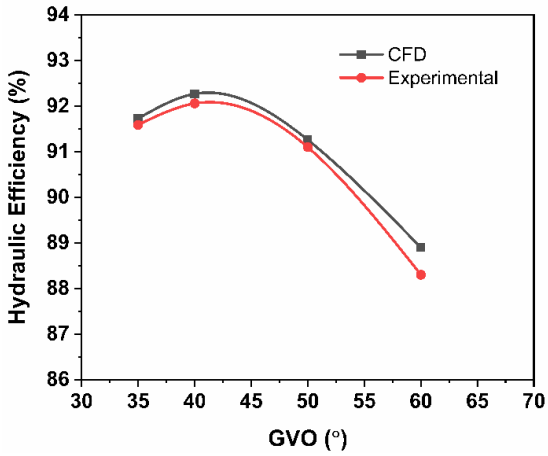

Figure 4. Variations of hydraulic efficiency at different GVO

Effect of cavitation on blade loading

Since the power developed by the turbine depends on the pressure distribution around the blade surface. The distribution of pressure on the surface of runner blade for cavitating and non-cavitating analysis has been determined using the blade loading curve at the mid-span of runner blade from the leading edge (LE) to the trailing edge (TE). The static pressure at any point is determined in terms of pressure coefficient (C_P) on the mid-span of runner blade and the

graphical representation is illustrated in Figure 5.

It is observed that the developed stage of cavitation disturbs the flow field resulting in uneven distribution of pressure and deteriorating the performance. There is a gradual decrease of pressure from LE to TE due to the extraction of energy by the runner blade from the flowing water. The highest pressure was observed at the LE of runner blade on the pressure surface, while the lowest pressure was observed at the TE of runner blade on the suction surface. It is observed from the blade loading that the pressure difference between the suction side and pressure side decreases with an increase in GVO. This is due to the decrease in the net head with an increase in GVO.

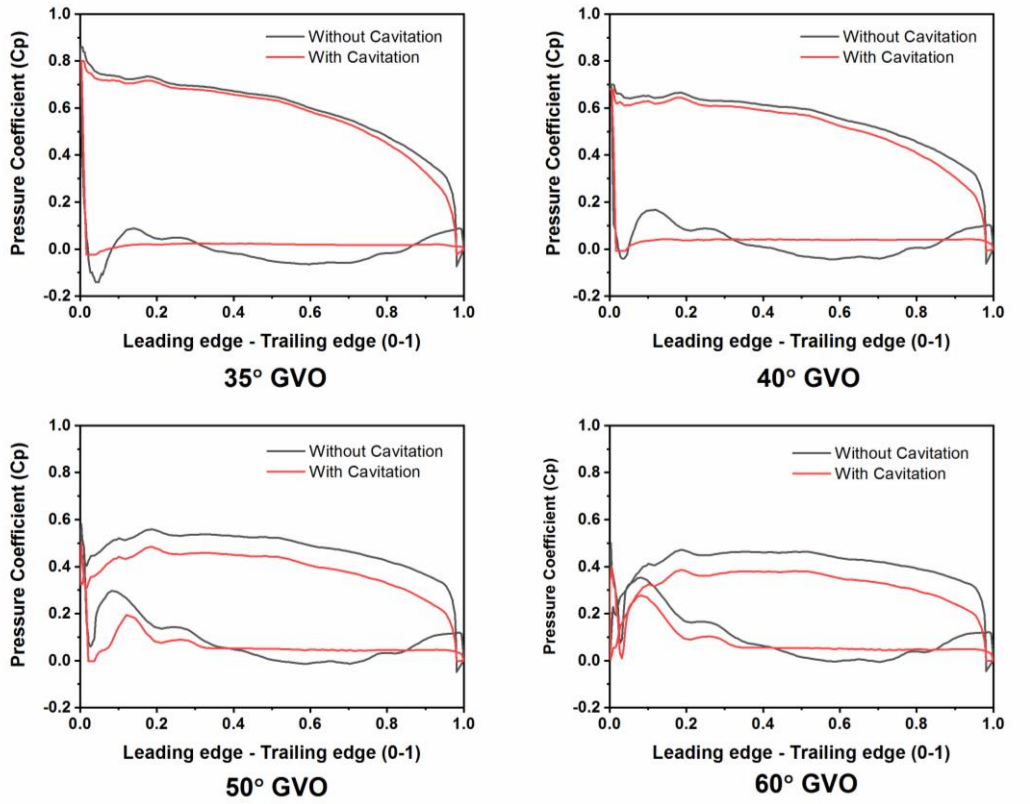

Figure 5. Pressure distribution at mid-span of runner blade surface

Computation of critical value of Thoma cavitation factor

Cavitation characteristics of Kaplan turbine are described by the “Sigma curve”. The value of Thoma cavitation factor for different outlet pressure is determined by Equation (2). The sigma curve is generally formed by varying the pressure at the draft tube outlet. The critical value of

Thoma cavitation factor is defined as a point on the sigma plot at which the hydraulic efficiency starts to drop from the hydraulic efficiency of non-cavitating.

In the present numerical flow simulation, the average static pressure at the outlet of draft tube is varied from 1 atm to 0.1 atm with the step of 0.1 atm and the σ values and hydraulic efficiency are computed. The sigma curve for 35º, 40º, 50º and 60º GVO are shown in Figure 6. As the static pressure at the draft tube outlet decreases, the value of σ will decrease. Initially, the hydraulic efficiency is nearly constant till the certain value of σ and afterward, the decrease in σ causes a drop in the hydraulic efficiency because of the mismatching of flow angle and the increase in losses and vibration due to collapsing of bubble. The value of critical cavitation factor is found to be 0.34, 0.39, 0.57 and 0.61 at 35º, 40º, 50º and 60º GVO and it is closely matched with the experimental values of 0.37, 0.42, 0.55 and 0.65 respectively. In order to avoid cavitation, the value of σ should always be greater than the σ_c.

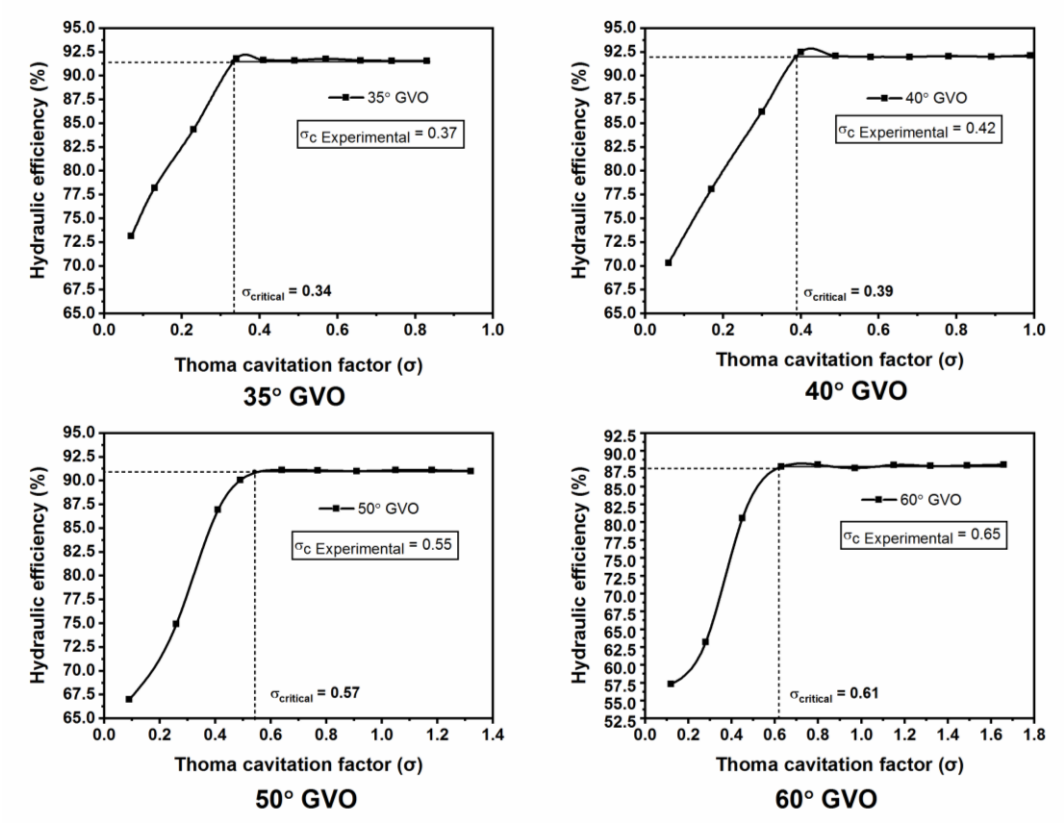

Figure 6. Sigma curve at different GVO

Effect of cavitation on flow parameters

The variations of mass averaged values of velocity coefficients (velocity normalized with the spouting velocity, i.e. $\sqrt{2gH}$) and flow angles with GVO for cavitating and non-cavitating conditions are shown in Figure 7. It is seen that the relative flow angles at the inlet are nearly the same at respective GVO in both cavitating and non-cavitating conditions. But the flow angles at the outlet are affected due to cavitation and decrease with an increase in GVO. The absolute and whirl velocity coefficients decrease from inlet to outlet, whereas relative velocity coefficients increase from inlet to outlet for both cavitating and non-cavitating conditions and confirm the characteristics of Kaplan turbine. It is also seen that the magnitude of relative and meridional velocity increases with the increase in GVO. The meridional velocity coefficient at the inlet and outlet of runner is nearly the same for non-cavitating at each GVO, but it increases from the inlet to outlet of runner for non-cavitating conditions due to the presence of vapour bubble and pressure fluctuation.

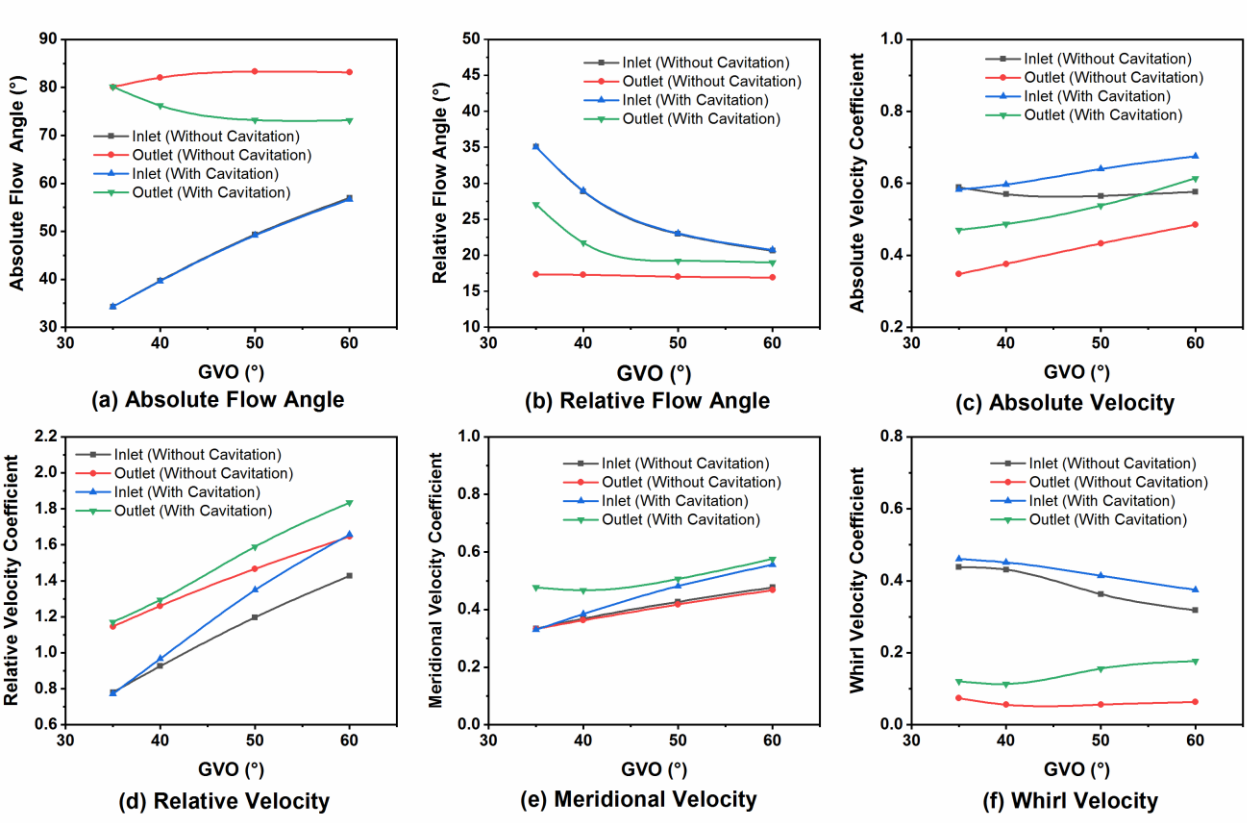

Figure 7. Variation of flow parameters for cavitating and non-cavitating conditions

Pressure contours

The pressure distribution on the surfaces of runner blade affects the development of force and torque. The variation of pressure on the suction surface of runner blades at different GVO for the developed stage of cavitation are shown in Figure 8. The pressure decreases from the inlet edge to outlet edge of runner due to flow acceleration. The pressure drops near the exit of runner and hence the suction surface of runner blades is more susceptible to cavitation. It is perceived from Figure 8 that the low-pressure zone on the suction surface sprayed the whole surface at lower GVO i.e. 35º and 40°. As the GVO increases to 50º and 60º, the pressure distribution becomes non-uniform, having higher pressure at the leading edge and lower pressure at the trailing edge. This may be due to increased water vapour volume fraction at higher GVO.

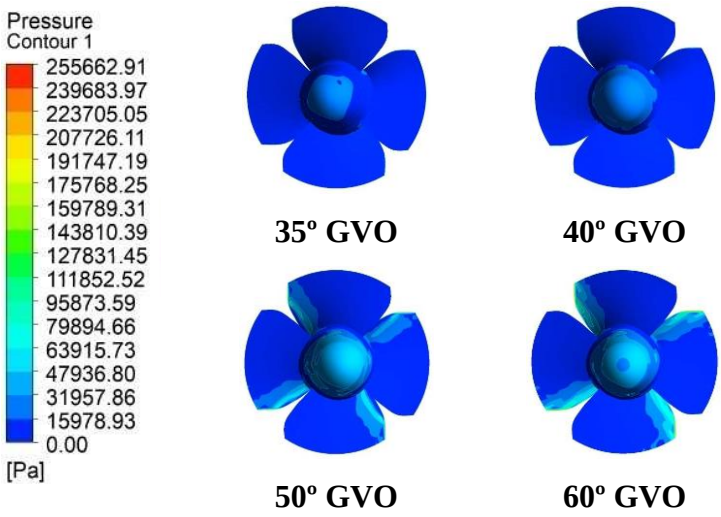

Figure 8. Variation of pressure on the suction surface of runner blades at different GVO for the developed stage of cavitation

Water vapour volume fraction distributions

The water vapour volume fraction distribution helps in the prediction of cavitation development on the runner blade surface. It described the fraction of water vapour distributed on the surface. The value of water vapour varies from ‘0 to 1′. A value ‘0′ indicates that there is no water vapour on the surface, while value ‘1′ indicates 100% water vapours on the surface. Various cavitation stages such as the initial, appreciable and developed cavitation stages have been observed for

different GVO. Figure 9 shows the development of water vapour volume fraction on the runner hub cone and suction surface of runner blades for different operating conditions.

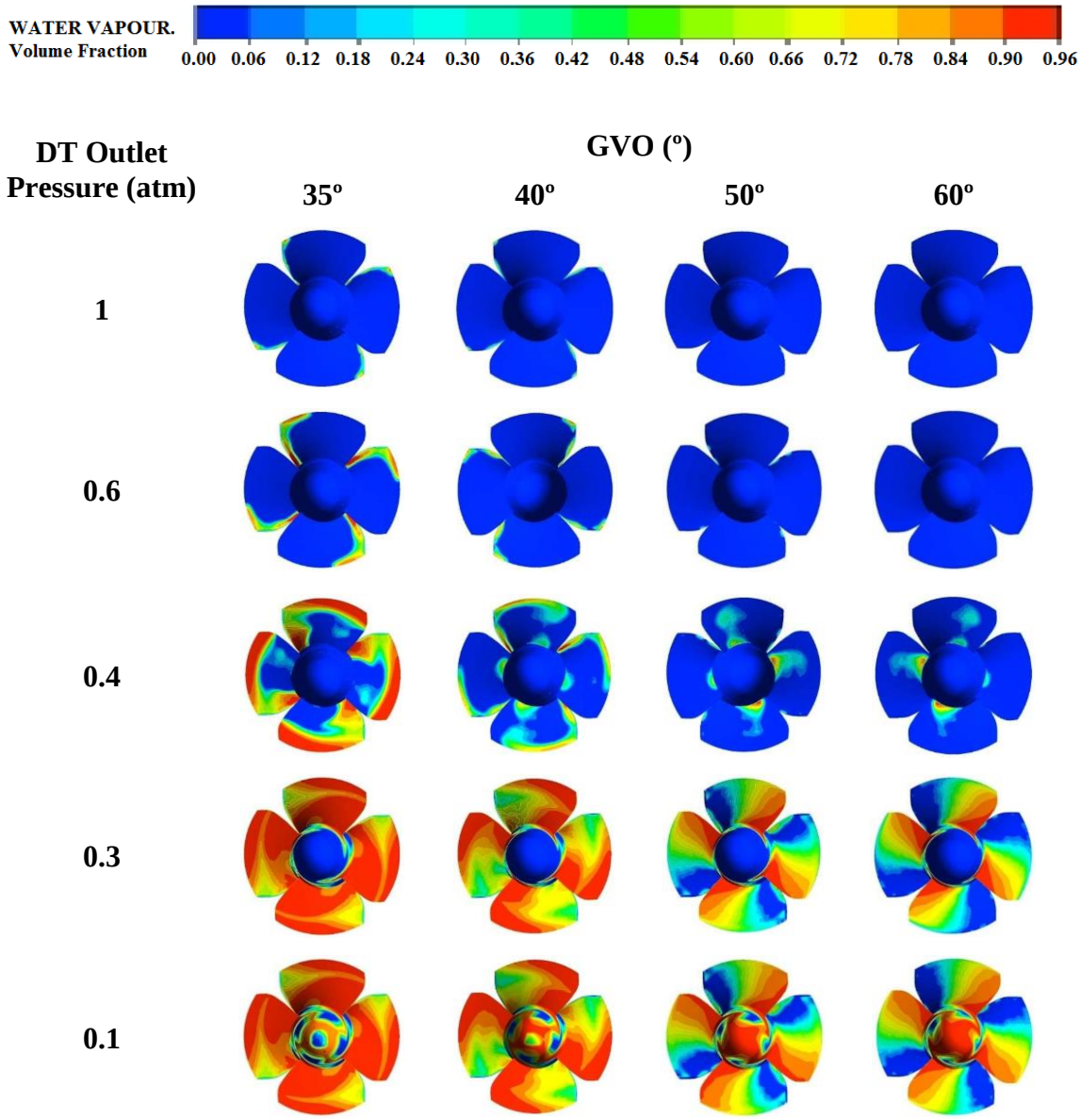

Figure 9. Water vapour volume fraction on the runner hub cone and suction surface of runner blades for different operating conditions

The amount of vapour volume fraction increases on the suction surface of runner with the decrease in pressure at the draft tube outlet. The water vapour volume fraction formation increases as the outlet pressure are below 0.4 atm and cover almost the entire space. It is seen that initially, there was no water vapour volume fraction on the runner blade surface, but

continues decrease in pressure at the draft tube outlet causes more pressure reduction at the runner outlet and this leads to increased water vapour volume fraction. As the GVO increases, the water vapour volume fraction shifts towards the trailing edge leading to more cavitation at the trailing edge.

CONCLUSIONS

The present investigation deals with the performance and cavitation characteristics of Kaplan turbine for the different working conditions. The steady-state numerical simulations have been carried out and the computed results are validated with the experimental model testing results. The hydraulic efficiency of CFD results is closely matched with the experimental results at 35º, 40º, 50º and 60º GVO for non-cavitating analysis. It is observed from the blade loading that the pressure difference between the suction side and pressure side decreases with an increase in GVO. The sigma curve is generated for different operating conditions to analyze the cavitation phenomenon and it is observed that the hydraulic efficiency slightly increases during the appreciable stage of cavitation due to the flow smoothing over the runner blades because of vapour bubbles present in flow. The value of critical cavitation factor is found to be 0.34, 0.39, 0.57 and 0.61 at 35º, 40º, 50º and 60º GVO and it is closely matched with the experimental values 0.37, 0.42, 0.55 and 0.65 respectively. The irregularities in flow and pressure fluctuations during developed cavitation greatly reduce the hydraulic efficiency of turbine. The velocity and flow angles at the inlet and outlet of runner are affected due to change in GVO and cavitation.

The present investigation is very realistic and related to the actual site conditions. This study will help the designer to obtain a more efficient and cavitation-free runner design for rated and off-design conditions. The findings of this investigation will help in the design, operation, and maintenance of Kaplan turbine. Further research will be conducted into material selection and design modification of runner blade to solve the problem related to the off-design operational conditions of the turbine, perhaps reducing the risk of cavitation.

REFERENCES

Brijkishore, Khare, R. & Prasad, V. 2021. Prediction of cavitation and its mitigation techniques in hydraulic turbines - A review. Ocean Engineering 221 (2021): 108512.

Brijkishore, Khare, R. & Prasad, V. 2020. Performance evaluation of Kaplan turbine with different runner solidity using CFD. In Advanced Engineering Optimization Through Intelligent Techniques, Springer, Singapore: 757–767.

Celebioglu, K., Altintas, B., Aradag, S. & Tascioglu, Y. 2017. Numerical research of cavitation on Francis turbine runners. International Journal of Hydrogen Energy 42 (28): 17771–17781.

Geng, L., Chen, J. & Escaler, X. 2020. Improvement of cavitation mass transfer modeling by including Rayleigh – Plesset equation second order term. European Journal of Mechanics / B Fluids 84 (2020) 313–324.

Jošt, D., Morgut, M., Škerlavaj, A., Nobile, E. 2015. Cavitation Prediction in a Kaplan Turbine Using standard and optimized model parameters. 6th IAHR International Meeting of the Workgroup on Cavitation and Dynamic Problems in Hydraulic Machinery and Systems, Ljubljana, Slovenia.

Kamal, M., Saini, G., Abbas, A. & Prasad, V. 2021. Prediction and analysis of the cavitating performance of a Francis turbine under different loads. Energy Sources, Part A: Recovery, Utilization, and Environmental Effects (2021): 1–25.

K**umar, D. & Bhingole, P.P. 2015.** CFD based analysis of combined effect of cavitation and silt erosion on Kaplan turbine. Materials Today: Proceedings 2 (2015) 2314 –2322.

Lal, J. 2011. Hydraulic machines. Metropolitan Book Co. Pvt. Ltd. Delhi.

Liu, Y., Wang, L. & Zhu, Z. 2016. Experimental and numerical studies on the effect of inlet pressure on cavitating flows in rotor pumps. Journal of Engineering Research 4 (2): 151–171.

Motycak, L., Skotak, A. & Kupcik, R. 2012. Kaplan turbine tip vortex cavitation-analysis and

prevention. IOP Conference Series: Earth and Environmental Science 15 (2012): 032060.

Nennemann, B. & Vu, T.C. 2007. Kaplan turbine blade and discharge ring. 2nd IAHR International Meeting of the Workgroup on Cavitation and Dynamic Problems in Hydraulic Machinery and Systems Timisoara, Romania 52 (66): 47–54.

Saini, G. & Saini, R.P. 2020. A computational investigation to analyze the effects of different rotor parameters on hybrid hydrokinetic turbine performance. Ocean Engineering. 199(2020): 107019.

Shamsuddeen, M.M., Park, J., Choi, Y.S. & Kim, J.H. 2020. Unsteady multi-phase cavitation analysis on the effect of anti-cavity fin installed on a Kaplan turbine runner. Renewable Energy 162(2020): 861–876.

Singh, V., Kumar, S. & Ratha, D. 2021. Experimental and Numerical analysis of Flow characteristics of sand water slurry in a horizontal pipe. Journal of Engineering Research 1–16.

Teran, L.A., Larrahondo, F.J. & Rodríguez, S.A. 2016. Performance improvement of a 500-kW Francis turbine based on CFD. Renewable Energy 96: 977–992.

Tiwari, G., Kumar, J., Prasad, V. & Kumar, V. 2020. Derivation of cavitation characteristics of a 3MW prototype Francis turbine through numerical hydrodynamic analysis. Materials Today: Proceedings 26(2020): 1439–1448.

Weili, L., Jinling, L., Xingqi, L. & Yuan, L. 2010. Research on the cavitation characteristic of Kaplan turbine under sediment flow condition. In IOP Conference Series: Earth and Environmental Science 12(2010): 012022.

Zhang, D., Shi, L., Shi, W., Zhao, R., Wang, H. & van Esch, B.P.M. 2015. Numerical analysis of unsteady tip leakage vortex cavitation cloud and unstable suction-side-perpendicular cavitating vortices in an axial flow pump. International Journal of Multiphase Flow 77: 244–259.

Zhang, Y., Liu, K., Xian, H. & Du, X. 2018. A review of methods for vortex identification in hydroturbines. Renewable and Sustainable Energy Reviews 81(2018): 1269–1285.